Hsp90 shapes adaptation by controlling the fitness consequences of regulatory variation

Christopher M. Jakobson[1,4], José Aguilar-Rodríguez[1,2,4], and Daniel F. Jarosz[1,3]*

[1]Department of Chemical and Systems Biology, Stanford University School of Medicine, Stanford, CA, USA

[2]Department of Biology, Stanford University, Stanford, CA, USA

[3]Department of Developmental Biology, Stanford University School of Medicine, Stanford, CA, USA

[4]These authors contributed equally.

*To whom correspondence should be addressed: jarosz@stanford.edu

ABSTRACT

The essential stress-responsive chaperone Hsp90 impacts development and adaptation from microbes to humans. Yet despite evidence of its role in evolution, pathogenesis, and oncogenic transformation, the molecular mechanisms by which Hsp90 alters the consequences of mutations remain vigorously debated. Here we exploit the power of nucleotide-resolution genetic mapping in *Saccharomyces cerevisiae* to uncover more than 1,000 natural variant-to-phenotype associations governed by this molecular chaperone. Strikingly, Hsp90 more frequently modified the phenotypic effects of *cis*-regulatory variation than variants that altered protein sequence. Moreover, these interactions made the largest contribution to Hsp90-dependent heredity. Nearly all interacting variants—both regulatory and protein-coding—fell within clients of Hsp90 or targets of its direct binding partners. Hsp90 activity affected mutations in evolutionarily young genes, segmental deletions, and heterozygotes, highlighting its influence on variation central to evolutionary novelty. Reconciling the diverse epistatic effects of this chaperone, synthetic transcriptional regulation and reconstructions of natural alleles by genome editing revealed a central role for Hsp90 in regulating the fundamental relationship between activity and phenotype. Our findings establish that non-coding variation is a core driver of Hsp90's influence on heredity, offering a mechanistic explanation for the chaperone's strong effects on evolution and development across species.

INTRODUCTION

The genotype-to-phenotype map is constantly remodeled by the environment and in response to stress[1], with strong impacts on development as well as in disease and evolution[2]. The Heat Shock Protein 90 kDa (Hsp90) chaperone has attracted keen interest as a candidate to enact such modifications of the relationship between genotype and phenotype[3,4]. Hsp90 is a 'hub of hubs' with very high genetic and physical connectivity[5]; its clients[6], enriched in kinases, ubiquitin ligases, and other signaling factors[7], are likewise highly connected nodes of regulatory networks. As a consequence, Hsp90 influences diverse properties of its client proteins, including protein turnover, steady-state levels, and localization[8]. Remarkably given its connectivity, the abundance and activity of Hsp90 varies substantially across environmental conditions[9]. These features endow Hsp90 with the capacity to control the relationship between activity and environmental stress for a network of functionally diverse regulatory proteins.

Hsp90 has profound impacts on the manifestation of the phenotypic effects of genetic variation[10–17]: modest impairment of Hsp90 function during development in *Drosophila melanogaster* results in pronounced changes to wings, eyes, and legs[15]. The lineage specificity of these developmental phenotypes[15,18], as well as those observed in other organisms[16], suggests that natural polymorphisms determine how Hsp90 shapes the developmental program. Multiple oncogenic[17] and drug-resistance[10] mutations, as well as other heritable traits in the wild[14], depend on Hsp90.

Despite considerable interest and study, how Hsp90 exerts such diverse effects remains uncertain. Prior studies have examined the interactions between Hsp90 and, variously, precise gene deletions[19,20], naturally segregating haplotypes[21], Fanconi anemia mutations[12], variants underlying Mendelian disorders[22], and genotypes harboring small numbers of nearly random mutations[11]. The underlying mutations whose effects are modified by Hsp90 have remained obscure in all but a handful of instances[12]. Moreover, because of Hsp90's role as a molecular chaperone, studies that focused on individual variants made the pragmatic assumption that chaperone inhibition primarily impacted coding variation. This gap in knowledge has left a wide gulf between examples of Hsp90's influence on the capacity of genetic variation to produce phenotypes and scant molecular understanding of how its chaperone activity is linked to these outcomes.

The molecular activity and clientele of Hsp90 are deeply conserved throughout Eukarya[23]. The advent of genetic mapping approaches in the budding yeast *S. cerevisiae* that dissect complex

traits to their underlying causal variants[24,25] thus presents a newfound opportunity to understand the influence of Hsp90 on heredity. Diverse collections of wild isolates[26,27], precision genome engineering tools[28], and comprehensive knowledge of the genetic and physical interactors of Hsp90[29,30], as well as the targets of key clients[31,32], make this an ideal venue to understand the mechanisms by which the chaperone network reshapes the genotype-to-phenotype map.

Here, we harness this system to identify thousands of natural polymorphisms throughout the genome whose effects depended strongly on Hsp90 function. Even though Hsp90 is a protein chaperone, these effects were most pronounced for non-coding variation. Nearly all interacting polymorphisms occurred in genes encoding Hsp90 client proteins, clients of co-chaperones, or the targets of regulatory proteins that depend upon Hsp90 to function. We also find evidence for potent modification of evolutionary trajectories by Hsp90: its inhibition altered the phenotypic effects of heterozygous mutations, natural segmental deletions, and mutations in evolutionarily young genes. Our results show that the Hsp90 chaperone network exerts a profound influence on the relationship between activity and phenotype, providing a mechanistic explanation for its potent impact on *cis*-regulatory variants and for the ubiquity of Hsp90-dependent phenotypes under stress and in development.

RESULTS

Nucleotide-resolution mapping of Hsp90-dependent phenotypes

To enable genetic mapping with high resolution and sensitivity, we employed ~15,000 fully genotyped progeny[24] from a cross between two wild *Saccharomyces cerevisiae* parents[25,33]: RM11, isolated from a California vineyard[34], and YJM975, isolated from an immunocompromised patient[35]. The paralogous genes encoding Hsp90—*HSC82* and *HSP82*—are not polymorphic in the mapping panel (mutations in these genes could confound mapping). To assess the chaperone's impact on the effects of natural variants [**Fig. 1A**], we used a potent and specific natural product inhibitor, radicicol[36], at a dose that reduced but did not eliminate Hsp90 activity[17] [**Fig. S1A**]. This degree of Hsp90 inhibition did not perturb growth in the absence of stress [**Fig. S1B**] nor induce a bounce-back heat shock response[21] [**Fig. S1CD**].

We examined the growth of the 15,000-isolate panel in response to diverse environmental perturbations (including alternate carbon sources, toxic metal ions, and DNA-damaging agents, as well as antifungal drugs used clinically and in agriculture) [**Supplementary Table S1**]. Parallel

experiments in the presence of radicicol revealed that Hsp90 inhibition dramatically altered the growth of many F_6 diploid progeny [**Fig. 1B**] and, moreover, did so in a manner that was highly specific to the environment [**Fig. S1E**]. Coarse genetic mapping readily identify loci with Hsp90-dependent phenotypic effects [**Fig. 1C**], including the rapamycin-resistance phenotype of a locus centered about the *AVO3* (*TSC11*/RICTOR[37]) gene [**Fig. 1D**].

To pinpoint the polymorphisms responsible for Hsp90-dependent traits, we performed high-resolution genetic mapping[25,33,38] of the change in growth upon chaperone inhibition. Based on over 1,000,000 growth measurements and a multivariate coarse- and fine-mapping procedure[24], we identified 1,154 Hsp90-dependent loci throughout the genome that could be resolved to a single variant, exceeding the number previously identified by orders of magnitude [**Supplementary File S1**]. In total, 806 genes were implicated in at least one interaction between a variant and Hsp90 inhibition. Although Hsp90 generally influenced homozygotes more strongly, we also observed 567 cases in which the chaperone affected a variant's dominance. Because most mutations originate as heterozygotes, this behavior, too, is likely an important facet of Hsp90's influence on natural genetic variation. More broadly, considering the modest number of conditions we surveyed in our experiments, the involvement of more than 10% of genes in Hsp90-dependent phenotypes emphasizes the widespread influence of Hsp90 on heredity.

We next classified interactions into two broad categories: buffering interactions, in which the phenotypic effect of an allele was masked by Hsp90 and *increased* upon radicicol treatment (decanalization[39] or the release of cryptic variation[40]); and potentiation interactions, in which the phenotypic effect of a variant was *reduced* when Hsp90 was inhibited (as with the transforming kinase v-Src[17]) [**Fig. S1F**]. Both types of interactions were common; buffering interactions were somewhat stronger than potentiations (median 15% larger; $p < 10^{-4}$) [**Fig. S1G**]. In addition to buffering and potentiation, we noted that several Hsp90-dependent effects *inverted* a variant's fitness. Although constituting a minority of the interactions we observed, the average effect size of such inversions was large [**Fig. S1H**] and may explain the 'line-crossing' Hsp90 dependence observed for randomly accumulated mutations[11]. Remarkably, Hsp90's impact on individual variants was comparable to the phenotypic contributions of the variants themselves [**Fig. S1I**]; all these effects were large relative to the threshold for selection in this organism ($s \sim 10^{-5}$ - 10^{-4})[41], suggesting that Hsp90 is poised to impact the evolutionary fate of a broad swath of natural genetic variation.

To confirm our statistical findings, we used genome editing to reconstruct the SNP in Avo3[42] linked to Hsp90-dependent rapamycin resistance [**Fig. 1E**]. Examining the AlphaFold model of this Hsp90 client[29], we noted that the polymorphic Lys1342 residue lay in the Avo3 C-terminus, which protects Tor2 from rapamycin[43], and is positioned to form a salt bridge likely disrupted by the Thr1342 substitution[44] [**Fig. 1F**]. Consistent with this hypothesis, the alternate Thr1342 allele found in the RM11 vineyard isolate conferred a pronounced fitness defect in rapamycin that was attenuated by radicicol treatment, whereas the Lys1342 allele found in the clinical isolate conferred potentiated resistance [**Fig. 1G**]. Neither variant strongly influenced growth in the absence of rapamycin [**Fig. S1J**] and we obtained similar results with the chemically distinct Hsp90 inhibitor geldanamycin[45], confirming that these phenotypes were transformed by Hsp90 activity.

To determine whether the effects of this variant were unique to these genetic backgrounds, we assessed the growth of 1,000 wild yeast isolates[27] under rapamycin treatment with and without Hsp90 inhibition. More than 100 of the wild strains bore the alternate Thr1342 allele, and the Hsp90-dependent effect of the polymorphism was apparent across this panel despite the presence of variation at more than one million other loci [**Fig. 1H**]. These data establish that, despite genetic background effects, results from our focused cross could be translated species-wide.

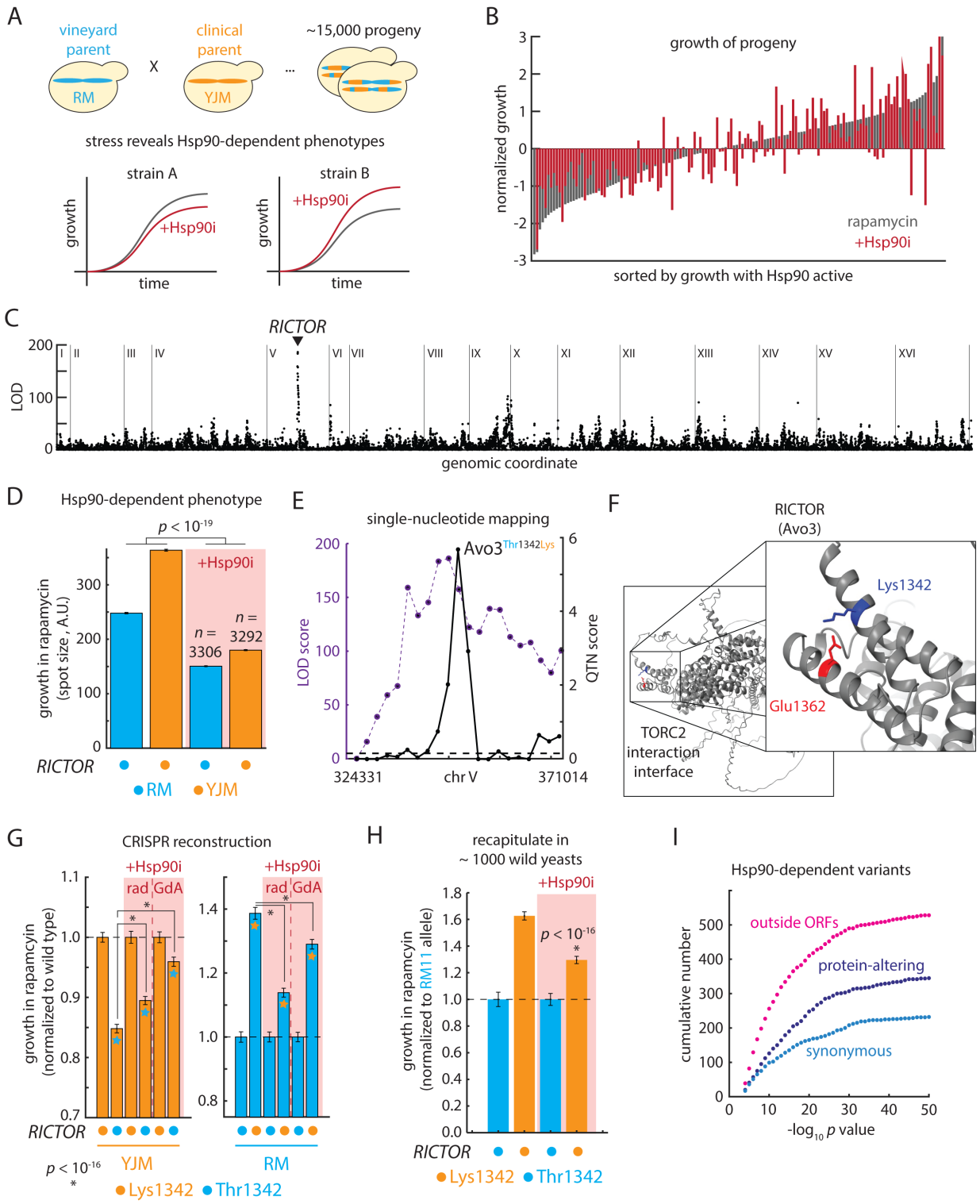

Figure 1. Identifying individual mutations underlying Hsp90-dependent phenotypes. (A) Schematic of genetic mapping population and hypothetical Hsp90-dependent phenotypes of different strains. (B) Normalized growth of randomly selected representative progeny in

rapamycin with Hsp90 active (grey) and inhibited with radicicol (red), sorted by growth with Hsp90 active. Shown are n = 146 randomly selected progeny. (C) Manhattan plot of univariate genetic mapping of Hsp90-dependent rapamycin resistance. Loci are in genomic order, with chromosomes as indicated. A strong association at the *AVO3*/RICTOR locus is highlighted. LOD, log of the odds distribution. (D) Growth in rapamycin with Hsp90 active (no shading) and inhibited with radicicol (red shading) of strains bearing the sensitive (blue) and resistant (orange) alleles of Avo3/RICTOR. Data shown are mean and s.e.m.; number of progeny with each homozygous genotype is as indicated; F test p value from multivariate regression; n as indicated. (E) Univariate genetic mapping of Hsp90-dependent rapamycin resistance (LOD score; left ordinate) overlaid with multivariate fine-mapping (ANOVA QTN score; right ordinate) of the same phenotype, highlighting the causal variant $Avo3^{Thr1342Lys}$. (F) Alphafold2 predicted structure of Avo3, highlighting the causal residue $Avo3^{Lys1342}$ and its proximity to $Avo3^{Glu1362}$. (G) Growth in rapamycin of genome-edited strains with Hsp90 active (no shading) and inhibited (red shading). The left panel shows wild type YJM975 $Avo3^{Lys1342}$ and edited YJM975 $Avo3^{Thr1342}$ strains (blue stars); the right panel shows wild type RM11 $Avo3^{Thr1342}$ strains and edited RM11 $Avo3^{Lys1342}$ strains (orange stars). Hsp90 was inhibited with radicicol (rad) and geldanamycin A (GdA). Data shown are mean and s.e.m. normalized to the wild type; p values by two-sample t test; n = 96 per genotype. (H) Replication of the Hsp90-dependent phenotype in wild isolates sorted by their Avo3 genotype as indicated: $Avo3^{Thr1342}$ in blue (n = 152) and $Avo3^{Lys1342}$ in orange (n = 806). Growth was measured with Hsp90 active (no shading) and inhibited (red shading) Data shown are mean and s.e.m. normalized to the growth of the RM11 $Avo3^{Thr1342}$ allele; p value by two-sample t test relative to growth without radicicol. (I) Cumulative frequency plots of multivariate regression p values for protein altering (dark blue), synonymous (light blue), and regulatory (pink) Hsp90-modified variants.

Hsp90 controls the phenotypic effects of regulatory variation

Although the Avo3 variant altered protein sequence, closer inspection of our mapping data revealed that nearly half (542 of 1,154) of the fine-mapped variants were outside of annotated open reading frames. Indeed, regulatory variants accounted for more Hsp90-dependent heredity than protein-altering variants [**Fig. 1I**; **Fig. S1K**], even though only 30% of the yeast genome is noncoding. To better understand this surprising enrichment, we first investigated a T>C variant 206 base pairs upstream of the *ERG11* transcription start site[46] [**Fig. 2A**] linked to Hsp90-buffered resistance to the antifungal drugs tebuconazole and fluconazole, which inhibit Erg11 and are widely used in agriculture[47] and the clinic[48]. Genomic reconstruction of the regulatory SNP recapitulated its buffered fitness effect [**Fig. 2B; Fig. S2A**]; the mutation had a negligible effect on growth in the absence of drug, regardless of Hsp90 activity [**Fig. S2B**]. These data establish that the buffered azole resistance was due to a regulatory variant rather than linked coding mutations.

We next examined the position of regulatory variants affected by Hsp90 relative to the transcriptional start sites (TSS) of the nearest genes. The largest and most frequent effects arose from variants immediately upstream of the TSS, consistent with altered transcription factor recruitment or transcription initiation. 123 Hsp90-dependent variants, however, were in the predicted 3' UTR of mRNAs and 55 in the 5' UTR [**Fig. 2C**], suggesting an important role for post-transcriptional regulation. Indeed, numerous Hsp90-dependent phenotypes arose from the 3' UTR of the cysteine desulfurase gene *NFS1*, which exhibits nutrient-dependent RBP binding[49]. Introducing a G>A polymorphism 61 base pairs downstream of *NFS1* into the YJM975 genetic background conferred pronounced buffered sensitivity to fluconazole and concomitant buffered resistance to the DNA-damaging agent doxorubicin, confirming the role of this 3' UTR in chaperone-dependent heredity [**Fig. 2D**]. Interestingly, we previously implicated coding variation at *NFS1* in buffered rapamycin resistance[21], suggesting that Hsp90-dependence may be a general property of variation at this gene. More broadly, our data demonstrate that the fitness effects of *cis*-regulatory variation alone can be potently controlled by the Hsp90 foldase.

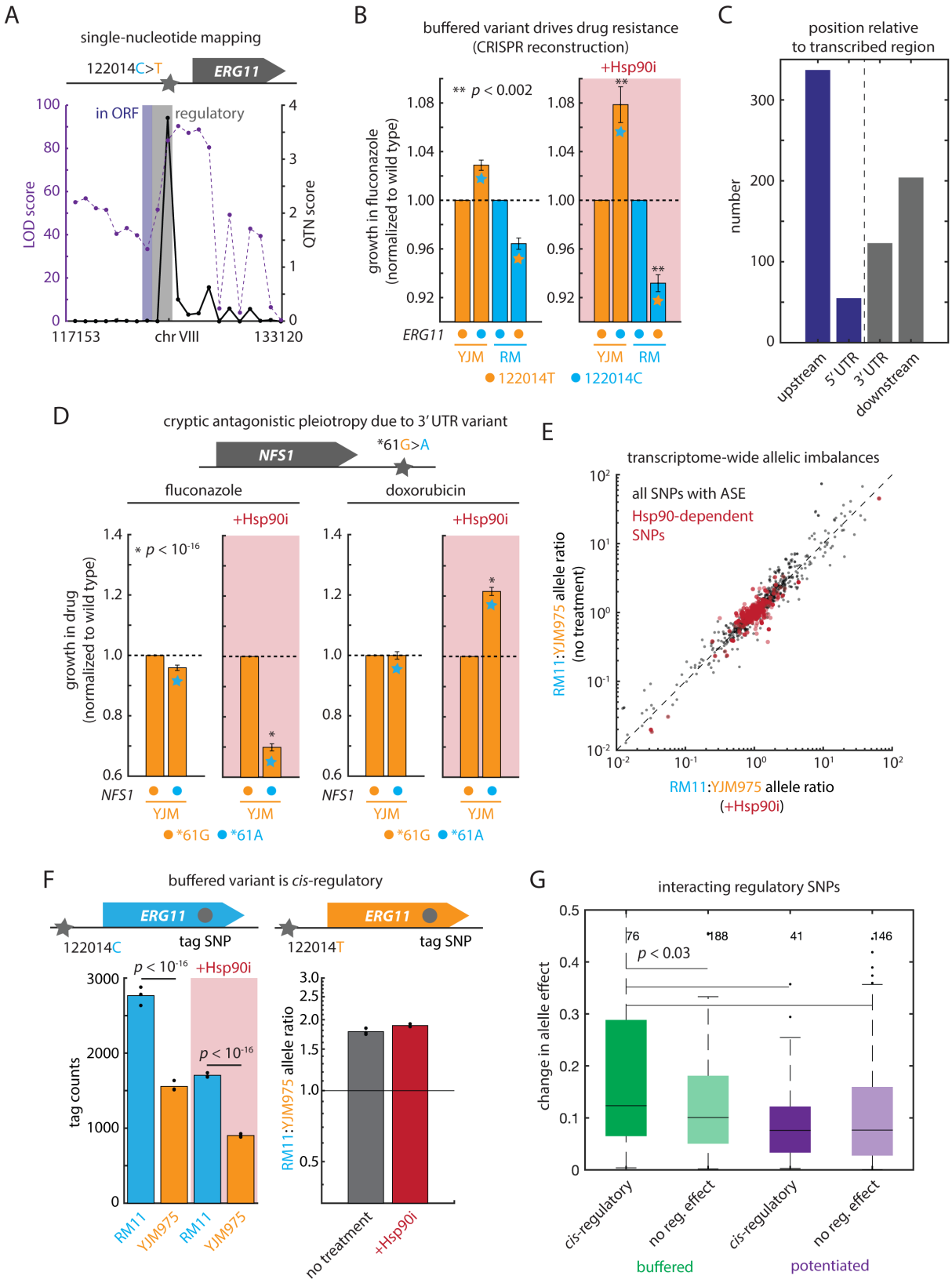
A
single-nucleotide mapping
122014C>T
ERG11
in ORF
regulatory
LOD score
QTN score
117153
chr VIII
133120
B
buffered variant drives drug resistance
(CRISPR reconstruction)
+Hsp90i
** p < 0.002
growth in fluconazole
(normalized to wild type)
ERG11
YJM
RM
122014T
122014C
C
position relative
to transcribed region
number
upstream
5′UTR
3′UTR
downstream
D
cryptic antagonistic pleiotropy due to 3′UTR variant
NFS1
*61G>A
fluconazole
doxorubicin
+Hsp90i
* p < 10^-16
growth in drug
(normalized to wild type)
NFS1
YJM
*61G
*61A
E
transcriptome-wide allelic imbalances
all SNPs with ASE
Hsp90-dependent
SNPs
RM11:YJM975 allele ratio
(no treatment)
RM11:YJM975 allele ratio
(+Hsp90i)
F
buffered variant is cis-regulatory
ERG11
122014C
122014T
tag SNP
p < 10^-16
+Hsp90i
tag counts
RM11
YJM975
RM11:YJM975 allele ratio
no treatment
+Hsp90i
G
interacting regulatory SNPs
p < 0.03
76
188
41
146
change in alelle effect
cis-regulatory
no reg. effect
buffered
potentiated

Figure 2. Hsp90 controls the phenotypic outcomes of *cis*-regulatory variation. (A) Univariate genetic mapping of Hsp90-dependent fluconazole resistance (LOD score; left ordinate) overlaid with multivariate fine-mapping (ANOVA QTN score; right ordinate) of the same phenotype, highlighting the causal variant *ERG11*$^{122014C>T}$. Indicated are a SNP in the *ERG11* ORF (blue shading) and SNPs in the associate regulatory region (grey shading) (B) Growth in fluconazole of genome-edited strains with Hsp90 active (no shading) and inhibited with radicicol (+Hsp90i; red shading). Each panel shows wild type YJM975 *ERG11*^{122014T}, edited YJM975 *ERG11*^{122014C} (blue stars), wild type RM11 *ERG11*^{122014C}, and edited RM11 *ERG11*^{122014T} (orange stars) strains. Data shown are mean and s.e.m. normalized to the wild type; *p* values by two-sample *t* test against the same mutant strain without radicicol treatment; $n = 384$ per genotype. (C) Frequency of Hsp90-modified regulatory variants occurring, respectively, upstream of the TSS, downstream of the TSS (5' UTR), upstream of the TES (3' UTR), and downstream of the TES for the nearest gene(s). (D) Growth in fluconazole (left) and doxorubicin (right) of genome-edited strains with Hsp90 active (no shading) and inhibited with radicicol (+Hsp90i; red shading). Each panel shows wild type YJM975 *NFS1*^{*61G}, and edited YJM975 *NFS1*^{*61A} (blue stars) strains. Data shown are mean and s.e.m. normalized to the wild type; *p* values by two-sample *t* test against the same mutant strain without radicicol treatment; $n = 384$ per genotype. (E) Allelic ratio (RM counts/YJM975 counts) in the hybrid diploid with Hsp90 inhibited by radicicol (abscissa) or with Hsp90 active (ordinate) for all SNPs with genome-wide significant allele-specific expression (grey) and for SNPs with Hsp90-dependent phenotypic effects (red). Data shown are mean allelic ratios across three replicates for each condition. (F) Top: Schematic of *ERG11* alleles in the hybrid diploid; indicated are the Hsp90-dependent 122014C>T regulatory variant and the Erg11^{Lys433Asn} tag SNP. Below left: estimated counts at Erg11^{Lys433Asn} tag SNP for the RM11 allele (blue) and the YJM975 allele (orange) with Hsp90 inhibited with radicicol (red shading) or Hsp90 active. Bars show mean and dots show replicates. Below right: Mean allelic ratio (RM11 counts/YM975 counts) at the Erg11^{Lys433Asn} tag SNP with Hsp90 inhibited with radicicol (red) or Hsp90 active (grey). Bars show mean and dots show replicates; *p* values by binomial test; $N = 3$. (G) Absolute change in allele effect for Hsp90-modified regulatory variants that were buffered (green) and potentiated (purple), sorted by whether the transcript exhibited allele-specific expression (left) or had a tag SNP but no allele-specific expression (right). Box plots show the median and upper and lower quartiles; whiskers show 1.5 times the interquartile range; *p* values by two-sample *t* test; *n* as indicated.

Allelic imbalance is invariant to Hsp90 activity

To better understand the molecular origins of the phenotypic interactions between Hsp90 and natural regulatory variants, we performed allele-specific mRNA sequencing of the heterozygous diploid parent of our genetic mapping panel. This approach capitalizes on polymorphisms in transcribed regions that 'tag' transcripts as originating from either the RM11 or YJM975 parental chromosomes [**Fig. S2C**]; a predominance of one haplotype over the other indicates the presence of a *cis*-acting regulatory variant at that gene[50]. Of the 451 phenotypic interactions between non-coding variants and Hsp90 in our mapping experiments, 107 (26%) exhibited significant allele-specific expression (ASE) under radicicol treatment (Bonferroni-corrected $q < 0.05$; see **Methods**, **Fig. S2D**, and **Supplementary File S2** for details and power calculations). We first hypothesized that Hsp90 inhibition might alter effects of these interacting SNPs on mRNA levels, causing their phenotypic effects to change. Yet to our surprise, allelic ratios were largely unchanged by Hsp90 inhibition across all segregating polymorphisms, whether or not their phenotypic effects depended on the chaperone [**Fig. 2E**; **Fig. S2E**]. The buffered variant at *ERG11*, for instance, showed pronounced RM11-biased expression (mean RM:YJM allelic ratio = 1.78), consistent with our observation that the RM11 allele conferred azole resistance [**Fig. 2F**], but this ratio was unchanged when Hsp90 was inhibited.

We did note, however, that the overall level of *ERG11* expression was markedly decreased by radicicol treatment. This observation led us to hypothesize that Hsp90 might control allele-specific fitness consequences without impacting the mRNA allelic ratio simply by altering the amount of folded, active protein in *trans*. Such a model would predict that Hsp90 would have a larger phenotypic effect on variants with greater allelic imbalance. Indeed, despite having little effect on mRNA ASE itself, Hsp90 more strongly impacted the consequences of variants with significant allelic imbalances ($p < 0.01$) [**Fig. S2F**]. Moreover, if most proteins are present at levels that do not limit growth under most conditions[51], then we might expect such interactions to be predominantly buffered; buffering interactions were stronger than potentiations for variants associated with mRNA *cis*-regulation ($p < 0.03$) [**Fig. 2G**; **Fig. S2G**]. Studies in diverse organisms have illustrated the potential for Hsp90 to have profound and lineage-specific consequences for development[16], often resulting in the release of cryptic phenotypic variation. Our results suggest that these interactions could arise from the confluence of *cis*-acting variants with *trans* effects that depend on Hsp90 activity.

Hsp90 modifies variation in direct clients and their targets

Our observation that coding and non-coding variants drove Hsp90-dependent phenotypes led us to ask whether either were linked directly to Hsp90's well-characterized chaperone activity or instead were connected by effects that percolated through the protein-protein interaction network. Strikingly, modified alleles were much more like to occur in genes encoding Hsp90 clients[29] ($p <$ 0.0007 for both Hsp82 and Hsc82) [**Fig. 3A**][9]. Because multiple chaperones are often involved in folding, we also searched the clientele of the Hsp70 family of chaperones, which collaborate with Hsp90[52,53]; these clients were also enriched for modified alleles ($p < 10^{-6}$ for Ssa1/2; $p < 0.01$ for Ssa4) [**Fig. 3A**]. Notably, although the Hsp90-dependent phenotypes we identified were mechanistically diverse and often driven by *cis*-regulatory variation, protein-folding activity directly connected Hsp90 and Hsp70 to the majority (59.8%) of interacting variants.

To investigate percolating effects [**Fig. 3B**], we examined the targets of three classes of regulatory proteins that are prominent amongst Hsp90's clientele: kinases, transcription factors (TFs), and E3 ubiquitin ligases. We first assessed which kinases might connect Hsp90 inhibition to changes in the effects of natural variants, identifying eighteen kinases whose targets[31] were enriched for Hsp90-dependent variation (Bonferroni-corrected q value < 0.05) [**Fig. 3C, Fig. S3A**]. Twelve interact with Hsc82 or Hsp82[54], indicating a potential mechanism for the modification of variants in their clients. Ninety-two predicted targets of the client MAP kinase Slt2, for example, bore interacting alleles[55]. The targets of the eighteen enriched kinases accounted for another 32.2% of the interacting alleles in our experiments. Thus, a total of 92.0% of Hsp90-dependent variants were connected directly *via* chaperone activity or *via* kinases, a deeply conserved class of Hsp90 client proteins.

We next asked whether Hsp90's phenotypic effects might likewise percolate through TFs and ubiquitin E3 ligases. Modified variants were enriched at the targets of five TFs [**Fig. 3C;** see **Methods**][32] but not amongst the physical interactors of E3 ligases[54] [see **Methods**], perhaps because the substrate specificity of E3 ligases remains poorly characterized[56]. These results suggest that, first, although the influence of Hsp90 on the genotype-to-phenotype map is complex, it is interpretable based on our knowledge of the functional roles of Hsp90, its close collaborator Hsp70, and key categories of client proteins. Second, the position of Hsp90 as a hub of hubs facilitates the simultaneous modification of alleles throughout a complex regulon attributable to

both direct and second-order interactions. Indeed, multiple mechanisms may converge on a single protein: many interacting alleles at direct clients were also *trans* targets of client regulators. Finally, the effects of Hsp90 are similarly likely to reach both regulatory and coding variation at the members of this diverse regulon.

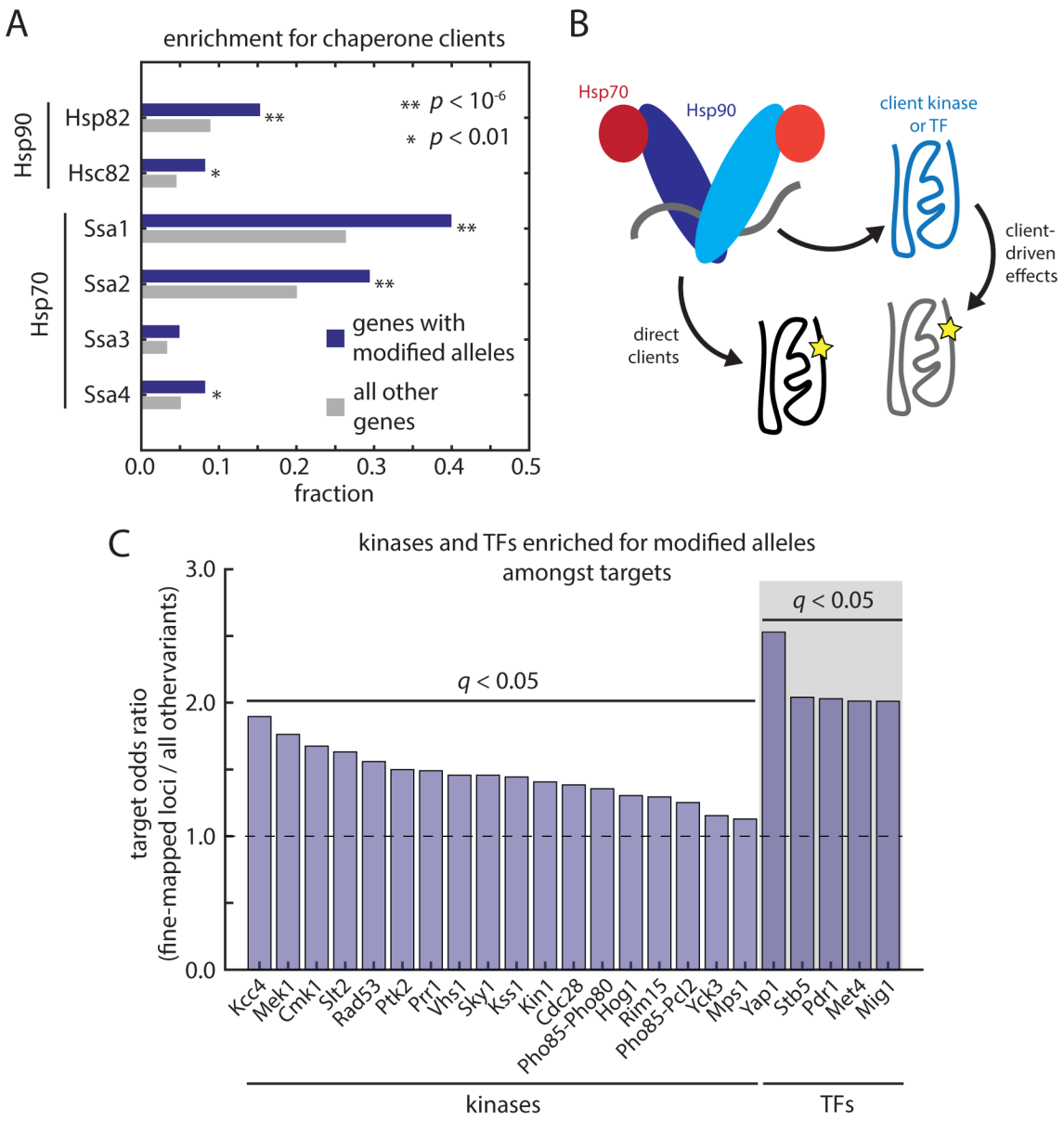

Figure 3. Hsp90-dependent phenotypes arise from chaperone clients and the targets of client regulatory proteins. (A) Fraction of genes bearing Hsp90-modified alleles (blue) and all other genes (grey) that are clients of the indicated chaperones. *p* values by Fisher's exact test. (B) Schematic of direct and indirect interactions between the Hsp90/70 chaperone network and mutated gene products. (C) Odds ratio that Hsp90-modified variants lie amongst the targets of the indicated kinases (left) and lie amongst the targets of the indicated sequence-specific TFs (right; grey) relative to all other segregating variants. *p* values by Fisher's exact test; shown are kinases and TFs with Bonferroni-corrected $q < 0.05$.

The influence of Hsp90 on complex heredity

Our mapping approach provided a comprehensive picture of Hsp90-dependent heredity, revealing that up to 90.0% of Hsp90's effect on fitness was due to changes in the phenotypic effects of genetic variants (median of 55.7% across all traits) [**Fig. S4A**]. Consistent with the widespread reservoir of co-regulated variants under the influence of Hsp90 activity, the Hsp90-dependence of phenotype was often genetically complex—the median trait comprised 142 modified alleles [**Fig. S4B**]. Hsp90-dependent growth in maltose, for example, depended on three separate large-effect alleles segregating at the *MAL1*, *MAL3*, and *GAL10* loci. The modified loci at *MAL3* and *GAL10* included regulatory variants, but a large-effect buffered locus at *MAL1* was due to a deletion encompassing three maltose metabolic genes: *IMA1, MAL11*, and *MAL13*[57]. The segmental deletion was much more deleterious to growth in maltose when Hsp90 was inhibited [**Fig. S4C**].

These joint interactions resulted in a remarkably environment-specific effect of Hsp90 inhibition on fitness [**Fig. S4D**]; despite Hsp90's pronounced impact in maltose, the three loci had negligible Hsp90 dependence in raffinose [**Fig. S4E**]. This was a general property of Hsp90-dependent heredity in our experiments: the effect of Hsp90 inhibition on the phenotypic consequences of variation was uncorrelated between different stress conditions [**Fig. S4F**]. To better understand how Hsp90 influenced the concerted effects of multiple variants, we examined how chaperone inhibition impacted the fitness of the eight possible combinations of homozygous genotypes at these three loci. The three simultaneous interactions altered the connectivity of the phenotypic landscape in maltose: several mutational steps were permitted (did not significantly decrease fitness) exclusively when Hsp90 was either fully active or inhibited [**Fig. 4A**]. This in turn altered the mutational paths accessible between genotypes without a stepwise decrease in fitness [**Fig. 4B**]. Simultaneously, Hsp90 inhibition coarsened the landscape: the effect of single-mutation steps in this mutational neighborhood was increased when Hsp90 was inhibited in maltose, in contrast to the same mutational neighborhood in raffinose [**Fig. 4C**]. The same was true under fluconazole treatment, in which variants at *ERG11*, *PDR1*, and *GRE2* were buffered [**Fig. 4D**]. These results illustrate how Hsp90 inhibition under stress can affect polygenic adaptation when the effects of multiple segregating polymorphisms are altered. By opening or foreclosing paths in the mutational space, chaperone activity shapes the tradeoff between metabolic specialization and the accessibility of other phenotypes when the environment changes.

The identification of interacting variants not only at the *MAL* but also the *FLO* genes, young, rapidly evolving subtelomeric gene families with highly variable gene content across *S. cerevisiae*[58] [**Supplementary File S1**], prompted us to ask if evolutionarily young genes, as a group, were predisposed to harbor Hsp90-dependent variation. After stratifying all *S. cerevisiae* genes by evolutionary age[59] [**Fig. 4E**], we found that the youngest genes harbored alleles that exhibited the strongest Hsp90-dependent phenotypic effects [**Fig. 4F**]. Moreover, this enrichment was driven predominantly by regulatory variation [**Fig. 4G**] and strong buffering interactions [**Fig. S4G**]. Thus, Hsp90-buffered variation provides a potent reservoir of phenotypic novelty, particularly at genes that contribute to niche-specific adaptation and harbor more condition-specific alleles of large effect[58].

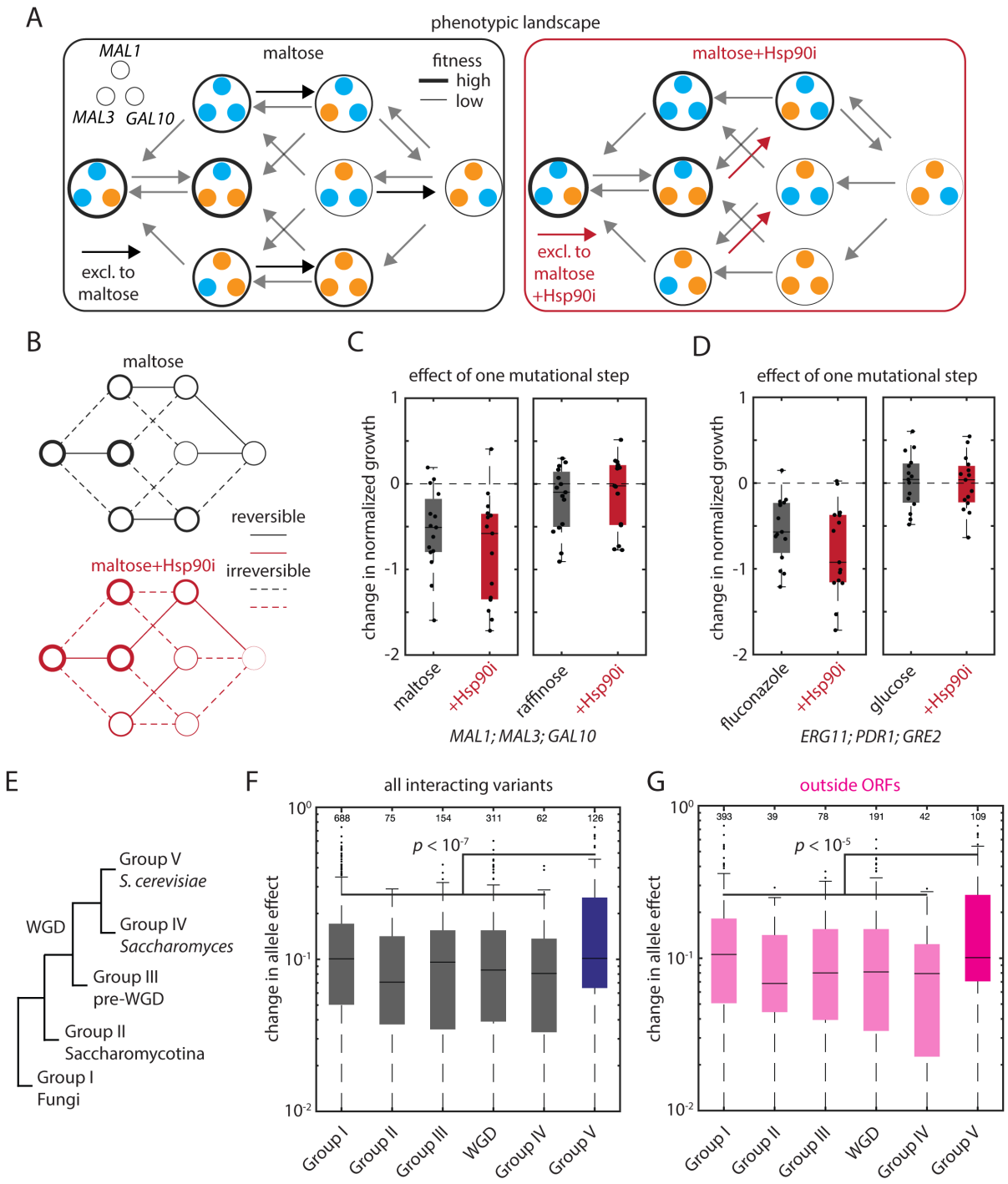

Figure 4. Complex genetic architectures of Hsp90-dependent heredity. (A) Phenotypic landscape of growth in maltose (left) or maltose with radicicol (right). Genotypes at *MAL1, MAL3,* and *GAL10* are as indicated; the fitness of each genotype is encoded in the line width of the enclosing circle. Grey arrows indicate permissible mutations that do not significantly decrease fitness (nominal $p > 0.05$) in either condition; black arrows show mutations only permissible in

maltose; red arrows show mutations only permissible in maltose with radicicol. (B) Phenotypic landscapes with genotypes as in (A) simplified to highlight mutational paths accessible by drift (solid lines; reversible) and paths that alter fitness (dashed lines; irreversible). (C) Change in mean normalized growth on maltose for all possible single-mutation steps amongst *GAL10*, *MAL1*, and *MAL3* alleles without (black) and with (red; +Hsp90i) inhibition of Hsp90 by radicicol. Box plots show the median and upper and lower quartiles; whiskers show 1.5 times the interquartile range. (D) As in (C), but for *ERG11*, *PDR1*, and *GRE2* in fluconazole and glucose. (E) Schematic of phylogeny used to classify *S. cerevisiae* genes by their evolutionary age based on the presence or absence of homologues in the taxa shown. (F) Absolute change in allele effect for Hsp90-modified variants with ages as indicated. Box plots show the median and upper and lower quartiles; whiskers show 1.5 times the interquartile range; p value by two-sample t test of the indicated age group against all other variants. n as indicated. (G) As in (F), but only for Hsp90-modified variants outside of open reading frames.

A general model for buffering by Hsp90

How does Hsp90 simultaneously drive such diverse effects and affect the outcomes of coding and non-coding variation alike? We returned to two observations from genetic mapping: first, that Hsp70 and Hsp90's direct clients were enriched in interacting genes, and second, that regulatory variation, which does not alter protein sequence, was a driver of Hsp90-dependent heredity. These observations led us to hypothesize that Hsp90-dependence was often an intrinsic property of certain gene products, rather than a property of mutations that led one allele to become Hsp90-dependent.

To directly test this idea, we again revisited the buffered *ERG11* regulatory variant. Interestingly, genetic mapping also suggested a role for the neighboring Erg11$^{\text{Asn433Lys}}$ coding variant in azole resistance when Hsp90 was fully active. We hypothesized that due to a reduction in Erg11 activity upon Hsp90 inhibition, the effects of both variants would be buffered [**Fig. S5A**]. After constructing strains bearing each variant singly as well as a strain bearing both mutations, we found that, strikingly, the single and double mutants all exhibited buffered resistance to azoles ($p < 10^{-4}$; $p < 0.001$) [**Fig. S5BC**]. Thus, disparate mutations at the *ERG11* locus were similarly labile to Hsp90 perturbation. Moreover, cryptic phenotypes may be attributable to compound alleles at loci that are sensitive to Hsp90 activity.

We next sought to explain why the effects of these mutations were suppressed by Hsp90. Building on the observation that *cis*-regulatory variation was frequently buffered, we hypothesized that a nonlinear activity-to-fitness relationship could be responsible [**Fig. 5A**]. If many copies of a protein are improperly folded or aberrantly post-translationally modified, or if total expression is decreased, a *cis*-regulatory variant of constant molecular consequence will exhibit an increased fitness impact due to the increased local slope of the activity-fitness sigmoid. This sigmoidal relationship exists for combinations of mutations in proteins[60,62] and for combinations of *cis*-regulatory variants at different genes[61], and has two implications: the fitness effects of arbitrary perturbations to Erg11 activity should depend on Hsp90 activity, and reducing Erg11 activity should be buffered.

To test these predictions quantitatively, we used synthetic CRISPR interference[63] to reduce *ERG11* transcription in the YJM975 parent [**Fig. 5B**]. As compared to a non-targeting guide RNA, reducing *ERG11* transcription caused a dose-dependent sensitivity to fluconazole [**Fig. 5C**]. In turn, Hsp90 inhibition caused a progressively greater sensitivity concomitant with decreasing

ERG11 transcription ($p < 10^{-8}$) [**Fig. 5CD**]; that is, the phenotypic consequences of losing Erg11 activity were systematically buffered by Hsp90, just as we observed for natural variation. Reducing *ERG11* levels had no effect in the absence of azole, regardless of Hsp90 activity [**Fig. S5D**], and comparable results were obtained in the RM11 parent, indicating that the phenomenon was independent of the *ERG11* genotype [**Fig. S5E**].

Finally, we asked whether we could identify genes with a steep activity-fitness relationship that might be more prone to Hsp90-dependent buffering. We examined haploinsufficient genes—those whose heterozygous mutants affect the diploid—because reducing their expression by approximately one-half leads to an appreciable phenotype [**Fig. S5F**]. Indeed, mutations in these genes[64] had stronger Hsp90-dependent effects [**Fig. S5G**]. This did not arise simply because many haploinsufficient genes are also essential: essential genes that are not haploinsufficient did not exhibit this trend. Moreover, in concordance with our model, these enrichments arose exclusively amongst buffering interactions [**Fig. 5E**]. Intriguingly, human genes scored as more essential (based on the frequency of predicted loss-of-function mutants in gnomAD[65]) and human genes found to be haploinsufficient in embryonic stem cells[66] are also enriched for known Hsp90 interactors[67] [**Fig. 5F**]. These genes may likewise be candidates to harbor Hsp90-buffered genetic variation arising from a sigmoidal activity-fitness relationship.

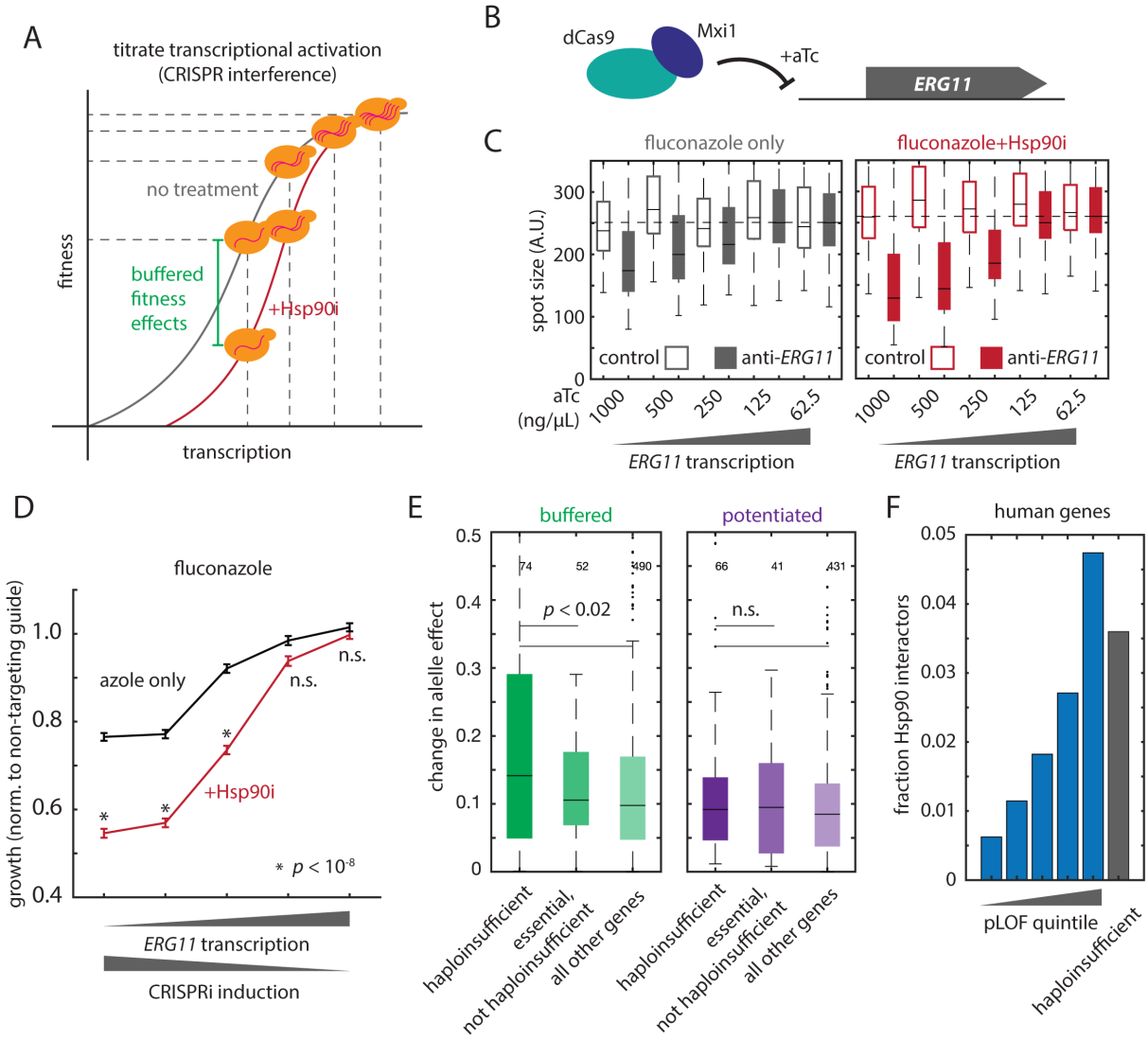

Figure 5: Hsp90 modifies the activity-fitness relationship. (A) Schematic of the effect of Hsp90 inhibition on fitness assuming a non-linear relationship between protein activity and phenotype. Increasing CRISPRi expression reduces *ERG11* expression; the fitness consequences of these changes are amplified when total activity is compromised by Hsp90 inhibition. (B) Schematic of CRISPR transcriptional interference mediated by a dCas9:Mxi1 fusion and anhydrotetracycline (+aTc) inducible gRNA. (C) Growth of YJM975 haploid strains expressing either a non-targeting control gRNA (open boxes) or an anti-*ERG11* gRNA (closed boxes) in fluconazole without the addition of radicicol (grey boxes) or with radicicol (red boxes). Shown is the concentration of inducing molecule (aTc) added to each culture. Box plots show the median and upper and lower quartiles; whiskers show 1.5 times the interquartile range; n = 384 per genotype. (D) Data in (C)

normalized to the growth of the YJM975 strain expressing the non-targeting control gRNA. Growth is in fluconazole without the addition of radicicol (black) or with radicicol (+Hsp90i; red). The concentrations of inducing molecule (aTc) added to each culture are (left to right) 1000 ng/µL, 500 ng/µL, 250 ng/µL, 125 ng/µL, and 62.5 ng/µL. Data shown are mean and s.e.m. (E) Absolute change in allele effect for Hsp90-modified variants in haploinsufficient genes, essential but not haploinsufficient genes, or all other genes, as indicated. Buffered interactions are shown at left (green) and potentiated interactions at right (purple). Box plots show the median and upper and lower quartiles; whiskers show 1.5 times the interquartile range; *p* values by two-sample *t* test; *n* as indicated. (F) Fraction of Hsp90-interacting gene products amongst all human genes, divided in quintiles by increasing gnomAD pLOF score (blue) and amongst genes haploinsufficient in embryonic stem cells (grey).

DISCUSSION

The influence of Hsp90 on the developmental and adaptive consequences of genetic variation has long been appreciated. However, aside from a handful of examples of mutations in client proteins, the molecular underpinnings of these effects have remained enigmatic. Here, our nucleotide-resolution approach revealed a surprise: *cis*-regulatory variants, which by definition do not alter protein stability, emerged as a driver of nearly half of Hsp90-dependent phenotypes. This behavior arose naturally from the chaperone's pervasive influence on activity-fitness relationships *via* direct clients and core regulatory proteins. Buffering interactions, which are enriched amongst these relationships, position Hsp90 to govern the release of cryptic, potentially adaptive variation in this regulatory circuitry. This mechanism combines the evolutionary advantages of *cis*-regulatory variation, which enables sophisticated spatiotemporal programming, with exquisite stress-dependent regulation of the Hsp90 chaperone machinery to release adaptive phenotypes under stress.

The preponderance of this behavior in the concise budding yeast genome suggests that interactions between Hsp90 and regulatory variation may be even more prominent in organisms with more elaborate regulatory architectures. Indeed, the pragmatic need for a low density of polymorphisms in our panel means that our results likely represent a lower bound on the prevalence of this phenomenon, even in yeast. Significant technical advances are still needed to understand Hsp90-dependent alleles of small effect and Hsp90-dependent genetic epistasis, both of which may play a role in Hsp90-dependent heredity. Nonetheless, even generous estimates of the contribution of epistasis suggest that, for some phenotypic transformations driven by the chaperone, other heritable variation that depends on Hsp90 activity (*e.g.* prions[68] or long-lived chromatin modifications[5]) may play an important role.

Our experiments identified numerous instances in which the impact of Hsp90 activity on fixed natural polymorphisms was as large as the effect of the variant alone. These were widespread throughout the genome, and although it is not straightforward to directly infer s from genetic mapping experiments, the effects we observed likely exceed the threshold for effective selection by multiple orders of magnitude. That many Hsp90-contingent effects were buffered and highly condition-specific further suggests a role in adaptation, particularly in rapidly changing environments. The environmental specificity of these interactions means that buffered variation can accumulate under normal conditions without compromising fitness. At the same time, this

variation is shaped by repeated selection that is only engaged when Hsp90 activity is compromised. This allows a greater diversity of genetic variation to persist in the population, broadening the accessible adaptive trajectories under stress. Moreover, by virtue of repeated cycles of selection, this reservoir of genetic potential may be predisposed to drive adaptive phenotypes.

Our results may also explain why Hsp90 inhibition has profound consequences for development, as the revelation of phenotypes due to *cis*-acting regulation are likely to have especially potent consequences in this context. Moreover, our observation that such variants were enriched in direct clients of Hsp90 and Hsp70, as well as their targets, suggests that these classes of proteins will be fertile ground to identify such interactions. Indeed, our data indicate that *cis*-regulatory variants controlling proteins already well-known to interact with Hsp90 may be especially profitable to explore.

Understanding how environmental change shapes Hsp90's clientele and the regulatory circuitry under its control is an intriguing area for future study. Nonetheless, our results suggest multiple potential advantages to an Hsp90-dependent activity-fitness relationship that incorporates regimes with varying slopes. This relationship buffers modest perturbations to activity but enhances the phenotypic consequences of large excursions; indeed, haploinsufficient genes may preferentially harbor buffered *cis*-regulatory effects. Our approach opens a path to ask whether other cellular components that are 'hubs of hubs' might also play important roles in the expression of genetic variation[4] and to characterize the spectrum of natural variants controlled by these factors.

Prior studies have indicated that Hsp90 facilitates the accumulation of coding variation in clients[69], accelerating their evolution[70]. Our findings suggest that the chaperone enables the accumulation of cryptic regulatory variation at these genes at least as strongly, providing an unappreciated and appealing potential mechanism for the influence of Hsp90 on developmental evolution in diverse systems from fruit flies to Mexican cavefish. Likewise, in cancer and in pathogens, the buffering of drug-resistant regulatory mutations by Hsp90 may allow their accumulation, subsequently being enriched amongst the surviving cells following treatment and promoting future drug-resistance. This, in turn, suggests that a paradigm that favors therapeutic Hsp90 inhibition, predicated on the Hsp90-addicted v-Src kinase, may be counterproductive if cryptic, buffered resistance is revealed and enriched. Distinguishing cases in which Hsp90 inhibition is helpful or deleterious to treatment is an important question for future investigation, as

is the relationship of an individual's reservoir of Hsp90-dependent buffering capacity with their polygenic risk for genetic disease. The decline of this buffering reservoir throughout lifespan may contribute to the emergence of pathologies with age.

Our findings address long-standing mechanistic questions surrounding the role of Hsp90 in transmuting genetic variation into selectable phenotypes. Hsp90's activity and connectivity with an expansive regulon of client proteins position it to control activity-fitness relationships throughout the core eukaryotic regulatory circuitry. In turn, the effects of numerous coding and regulatory variants simultaneously depend strongly on its stress-regulated activity. Finally, the acute environmental specificity of these buffered fitness effects facilitates their accumulation in advance of stress. Together, these features render Hsp90 a central governor of the critical evolutionary tradeoff between robustness and adaptability in the face of a changing environment, when diversification is most crucial.

ACKNOWLEDGMENTS

We thank Joseph Schacherer for the 1,002 Yeast Genomes Project strain collection, Justin Smith for the CRISPR interference plasmid, and the Jarosz Lab for critical feedback and advice. This work was supported by the NIH (DP2-GM119140, RF1-AG057334, R01-AG06341801, and R01-HG012366 to D.F.J.; F32-GM125162 to C.M.J.), the National Science Foundation (NSF-MCB116762 to D.F.J.), the Swiss National Science Foundation (P2ZHP3_174735 to J.A.-R.), the European Molecular Biology Organization (ALTF 724-2018 to J.A.-R.), a Searle Scholar Award (14-SSP-210 to D.F.J.), a Kimmel Scholar Award (SKF-15-154 to D.F.J.), a Vallee Scholar Award (to D.F.J.) and a Discovery Innovation Award from Stanford University (to D.F.J.). D.F.J. is also a Science and Engineering Fellow of the David and Lucile Packard Foundation. Some of the computing for this project was performed on the Sherlock cluster. We would like to thank Stanford University and the Stanford Research Computing Center for providing computational resources and support that contributed to these research results.

AUTHOR CONTRIBUTIONS

C.M.J., J.A.-R., and D.F.J. conceived the project. C.M.J. performed pilot, mapping, genome editing, phenotyping, and transcriptomic experiments, designed and implemented the genetic mapping pipeline, performed transcriptomic and bioinformatic analyses, and prepared the figures. J.A.-R. performed pilot experiments, designed genome editing reagents, and performed genome editing experiments. C.M.J. wrote the original draft of the manuscript. C.M.J. and D.F.J. reviewed and edited the manuscript with input from J.A.-R.

MATERIALS AND METHODS

Yeast strains

The construction and genotypes of the parents of the F_6 haploid collection, RM11 and YJM975, are described in She and Jarosz[25]. Briefly, the F_6 diploids used here were constructed by mating *leu⁻HYG*^{R} and *LEU*$^+$*hyg*^{S} F_6 haploid isolates genotyped previously[25] on YPD agar [RPI] followed by selection for diploidy on synthetic defined medium lacking leucine [Sunrise] and supplemented with 200 mg/L hygromycin. These F_6 diploids were arrayed into 384-well microtiter plates for cryostorage in SD-Leu+Hyg with 15% glycerol. All robotic manipulations were carried out using a Singer ROTOR pinning robot. The RM11 and YJM975 haploid parents of the original genetic cross bear auxotrophies used to facilitate crossing that are not present in the final F_6 diploid mapping panel. To avoid undesired interactions with these auxotrophies during validation experiments, reconstructions of Hsp90-interacting alleles were carried out in strains YDJ6635 (YJM975a from the SGRP haploid collection[26]) and YDJ6649 (a spore derived from diploid RM11a/α), both of which are auxotrophic only for uracil. Key yeast strains and plasmids are listed in **Supplementary Table S2**.

v-Src *assay for Hsp90 activity*

v-Src was expressed under the control of a galactose-inducible promoter from PDJ308 in the F_0 heterozygous diploid YDJ5924. Cells were grown on solid medium containing either 2% glucose (repressing) or 2% galactose (inducing) as the sole carbon source and with or without 10 μM radicicol; Images were cropped using custom R scripts and spot sizes were quantified using the *gitter* R package[71].

Western blotting

Cell lysis was conducted by bead beating in 20% trichloroacetic acid for 10 min at 50 Hz. Cell mass was normalized by optical density prior to lysis; approximately 1 OD-mL of cell mass was used per sample. Protein was precipitated for 30 min at ~23,000 x g at 4°C and the precipitate was resuspended in Tris pH 7.5 with 2% SDS before denaturation at 95°C for 5 min. Polyacrylamide gel electrophoresis was performed using 12-20% gradient gels at 120 V for 75 min. Proteins were transferred to PVDF membranes in Towbin transfer buffer for 2 hr at 100 V. Membranes were blocked with rehydrated milk, probed overnight at 4°C, and developed using WestFemto

chemiluminescent substrate. Matched gels loaded with equal sample volumes were stained with Coomassie brilliant blue in parallel to western blotting. When required for reprobing, membranes were stripped of primary and secondary antibodies by boiling in Tris-buffered saline for 5 min. Antibodies are listed in **Supplementary Table S4.**

Yeast culture conditions

Unless otherwise noted, yeast were propagated and phenotyped in minimal glucose medium consisting of 6.7 g/L yeast nitrogen base [RPI] and 20 g/L glucose [Sigma] supplemented with 20 mg/L uracil [Sigma] to satisfy the lone auxotrophy of the F_6 diploid panel. Prior to phenotyping experiments, diploid strains were revived from frozen stocks in liquid SD-Leu+Hyg medium in 384-well microtiter plates, propagated 24 hr at 30°C, then pinned to 1536-spot arrays on minimal glucose agar PlusPlates [Singer] and grown for 24 hr – 48 hr at 30°C. 1536-spot source plates prepared as described above were replicated to conditions as indicated using a Singer ROTOR pinning robot. Plates were incubated at 30°C and imaged at 24 hr intervals using an Epson V800 scanner. Images were cropped using custom R scripts and spot sizes were quantified using the *gitter* R package. Colony sizes were extracted for genetic mapping using custom MATLAB scripts. Working concentrations for the various environmental perturbations are described in **Supplementary Table S1**.

Genetic mapping

Prior to analysis, colony sizes were normalized to mean 0 and variance 1 (*i.e.* Z-scored) and filtered for outliers attributable to missing spots or debris (due to occasional pinning errors or image artifacts). Trait vectors were filtered for strains with an excess of missing genotypes and markers with insufficient genotype coverage were excluded. Statistical genetic mapping was performed essentially as described previously[24], with the difference that in the present work we mapped the change in the Z-scored trait for each segregant in each condition with and without 10 μM radicicol treatment. Briefly, coarse mapping was conducted by sequential stepwise selection on the homozygous followed by full (homozygous and heterozygous) genotype matrices. Fine mapping was conducted by ANOVA on *in silico* allele swaps as described in She and Jarosz 2018[25]. The genotype matrix included geometric pseudogenotypes corresponding to edge wells and to capture systematic plate-to-plate variability. Loci that were fine-mapped for one trait were inferred to be

the underlying causal variant for other traits in which they were the lead candidate. All trait and genotype data and the custom code used for mapping are available at https://github.com/cjakobson/mapping/tree/master/hsp90mapping and https://www.dropbox.com/scl/fo/aakdomnjk4rk949kvpsnw/h?rlkey=2vdos9m8dm3ybmkwcxm2ct8o6&dl=0 and summarized in **Supplementary File S1**.

Genome editing using CRISPEY

Oligonucleotides containing appropriate guide and donor sequences for CRISPEY editing were designed as described by Sharon and colleagues[28] using code provided in that study. Oligos were designed separately for RM11 to YJM975 and YJM975 to RM11 mutations to account for differences in guide and template sequences due to neighboring polymorphisms (**Supplementary Table S3**). SRR800790 and SRR1569760 were used as reference genomes for YJM975 and RM11, respectively. Gene editing was conducted largely as described in Sharon and colleagues[28]. Briefly, dsDNA was synthesized from oligos by PCR, dsDNA fragments were inserted into the NotI-digested PDJ2318 editing plasmid by isothermal assembly using a 2xHiFi Assembly kit, and the ligated DNA was transformed into chemically competent *E. coli*. Gene editing of yeast was performed by transformation of the editing plasmid and selection on SD-Ura followed by 24h of growth in synthetic galactose medium lacking uracil. From these editing reactions, yeast cells were streaked to single colonies on YPD plates followed by restreaking to 5-FOA plates to cure the editing plasmid. Single colonies were genotyped by PCR and Sanger sequencing of the desired edited locus; screening two colonies per edit was typically sufficient to recover an edited clone.

1002 Genomes yeast strains and phylogenetic analysis

Genotype information for the 1,002 Genomes collection and the corresponding yeast strains[27] were a generous gift of Joseph Schacherer (Univ. of Strasbourg). Frozen stocks were revived and phenotyping experiments performed as described above for the F_6 diploid mapping panel. Growth measurements and quantification were conducted by optical scanning of Singer PlusPlates using *gitter* and custom code as described above.

Allele-specific expression analysis

Cells were grown in triplicate in minimal media as described above with and without 10 μM radicicol and harvested at OD ~ 0.8-1.0. Cell pellets were snap-frozen and stored at -80°C before submission to BGI (www.bgi.com/us/home) for RNA extraction, polyA enrichment, reverse transcription, and sequencing. Transcript abundance was estimated using *kallisto*[72] and read counts per-site were estimated with *bcftools*[73] from *kallisto* pseudo-alignments. Allele-specific expression was called per-site based on a binomial test against the prior of major allele frequency = 0.5, with genome-wide Bonferroni correction based on the number of transcribed biallelic sites. Indels were excluded. After per-site calling, SNPs were assigned to genes and genes were assigned allelic imbalances if any SNP associated with their transcript exhibited significant allele-specific expression in any of the three replicate sequencing samples. Allelic imbalances agreed well between replicates [**Fig. S6**]. Results are summarized in **Supplementary File S2**. Sensitivity estimates were conducted based on a sliding simulated read depth followed by binomial tests, with mock Bonferroni correction performed assuming the true number of transcribed biallelic sites in the hybrid diploid.

Homozygous diploid mRNA sequencing

Cell were grown in triplicate in minimal media as described above with and without 10 μM radicicol and harvested at OD ~ 0.8-1.0. Cell pellets were snap-frozen and stored at -80°C before submission to BGI for RNA extraction, polyA enrichment, reverse transcription, and sequencing, as described above for allele-specific expression analysis. Transcript abundance was again estimated using *kallisto*. Transcripts per million (TPM) estimates agreed well between replicates [**Fig. S7**]. Results are summarized in **Supplementary File S3**.

CRISPR interference

CRISPRi plasmids were cloned as described in Smith *et al.* Briefly, the anti-*ERG11* guide RNA sequence was ordered as an ssDNA oligonucleotide and amplified using extension primers as described in[63]. The CRISPRi plasmid (p416gT-Gal4-dCas9-Mxi1) was opened with NotI and the anti-*ERG11* guide inserted by isothermal assembly using a 2xHiFi Assembly kit, and the ligated DNA was transformed into chemically competent *E. coli* to create PDJ2494. After transformation into *S. cerevisiae* alongside a matched control plasmid with a non-targeting gRNA (PDJ397), strains were pre-grown for 24 hrs in the appropriate concentration of anhydrotetracycline (aTc) to

establish steady-state knock-down then subjected to phenotyping under the appropriate aTc concentrations as described.

Bioinformatic resources and enrichment analyses

Genomic analyses used the *S. cerevisiae* R64 reference genome unless otherwise noted. Transcription start and end sites were retrieved from[74]. Targets of sequence-specific transcription factors were retrieved from[32]. Predicted kinase targets were retrieved from[31]. Enriched TF hits were logically connected to Hsp90 function: Mig1[75] and Pdr1[20] interact with Hsp90; Hsp90 inhibition downregulates Met4 targets[6]; and Yap1[76] and Stb5[77] homologues interact with Hsp90 in other species. Modified alleles at targets of Pdr1 and Stb5 were enriched for fitness effects in fluconazole, consistent with the role of these TFs in multidrug resistance. Although two E3 ligases (Rsp5 and Mpe1) exhibited modest enrichments, none were significant ($q < 0.05$) after multiple-testing correction. Gene and protein descriptions and GO terms were retrieved from SGD[54] and UniProt[78]. Predicted protein structures were retrieved from the AlphaFold Protein Structure Database[44]. Gene age estimates were retrieved from[59]. Haploinsufficient genes in *S. cerevisiae* were retrieved from[64]. pLoF data was retrieved from[65]. Haploinsufficient genes in human embryonic stem cells were retrieved from[66].

Strain and plasmid availability

The original F_6 haploid genetic mapping panel is available from the National Collection of Yeast Cultures and the F_6 diploid mapping panel and all other yeast strains described here are available upon request to Prof. Daniel F. Jarosz (jarosz@stanford.edu). Bacterial strains bearing plasmids used here are likewise available upon request. Various CRISPEY gene editing plasmids are available from AddGene.

Data and code availability

All data supporting the findings of this study are available within the paper and its Supplementary Information. All trait and genotype data required to recapitulate the mapping results are available at https://www.dropbox.com/scl/fo/aakdomnjk4rk949kvpsnw/h?rlkey=2vdos9m8dm3ybmkwcxm2ct8o6&dl=0. All custom genetic mapping code is available at

https://github.com/cjakobson/mapping/tree/master/hsp90mapping. RNA sequencing data are available at the Gene Expression Omnibus (GSE242925). Raw images of phenotyping experiments, custom code for cropping images and estimating spot sizes, and code for bioinformatic analyses and generating figures are available upon reasonable request to Prof. Daniel F. Jarosz (jarosz@stanford.edu).

REFERENCES

1. Cooper, D.N., Krawczak, M., Polychronakos, C., Tyler-Smith, C., and Kehrer-Sawatzki, H. (2013). Where genotype is not predictive of phenotype: towards an understanding of the molecular basis of reduced penetrance in human inherited disease. Hum. Genet. *132*, 1077–1130. 10.1007/s00439-013-1331-2.

2. Jablonka, E., and Lamb, M.J. (1998). Epigenetic inheritance in evolution. J. Evol. Biol. *11*, 159–183. 10.1046/j.1420-9101.1998.11020159.x.

3. Gee, Henry, Howlett, R., and Campbell, P. (2009). 15 Evolutionary Gems. Nature. 10.1038/nature07740.

4. Bergman, A., and Siegal, M.L. (2003). Evolutionary capacitance as a general feature of complex gene networks. Nature *424*, 549–552. 10.1038/nature01765.

5. Sawarkar, R., and Paro, R. (2013). Hsp90@chromatin.nucleus: an emerging hub of a networker. Trends Cell Biol. *23*, 193–201. 10.1016/j.tcb.2012.11.007.

6. Gopinath, R.K., You, S.-T., Chien, K.-Y., Swamy, K.B.S., Yu, J.-S., Schuyler, S.C., and Leu, J.-Y. (2014). The Hsp90-Dependent Proteome Is Conserved and Enriched for Hub Proteins with High Levels of Protein–Protein Connectivity. Genome Biol. Evol. *6*, 2851–2865. 10.1093/gbe/evu226.

7. Taipale, M., Krykbaeva, I., Koeva, M., Kayatekin, C., Westover, K.D., Karras, G.I., and Lindquist, S. (2012). Quantitative analysis of HSP90-client interactions reveals principles of substrate recognition. Cell *150*, 987–1001. 10.1016/j.cell.2012.06.047.

8. Csermely, P., Schnaider, T., So″ti, C., Prohászka, Z., and Nardai, G. (1998). The 90-kDa Molecular Chaperone Family: Structure, Function, and Clinical Applications. A Comprehensive Review. Pharmacol. Ther. *79*, 129–168. 10.1016/S0163-7258(98)00013-8.

9. Borkovich, K.A., Farrelly, F.W., Finkelstein, D.B., Taulien, J., and Lindquist, S. (1989). hsp82 is an essential protein that is required in higher concentrations for growth of cells at higher temperatures. Mol. Cell. Biol. *9*, 3919–3930. 10.1128/MCB.9.9.3919.

10. Cowen, L.E., and Lindquist, S. (2005). Hsp90 Potentiates the Rapid Evolution of New Traits: Drug Resistance in Diverse Fungi. Science *309*, 2185–2189. 10.1126/science.1118370.

11. Geiler-Samerotte, K.A., Zhu, Y.O., Goulet, B.E., Hall, D.W., and Siegal, M.L. (2016). Selection Transforms the Landscape of Genetic Variation Interacting with Hsp90. PLOS Biol. *14*, e2000465. 10.1371/journal.pbio.2000465.

12. Karras, G.I., Yi, S., Sahni, N., Fischer, M., Xie, J., Vidal, M., D'Andrea, A.D., Whitesell, L., and Lindquist, S. (2017). HSP90 Shapes the Consequences of Human Genetic Variation. Cell *168*, 856-866.e12. 10.1016/j.cell.2017.01.023.

13. Queitsch, C., Sangster, T.A., and Lindquist, S. (2002). Hsp90 as a capacitor of phenotypic variation. Nature *417*, 618–624. 10.1038/nature749.

14. Rohner, N., Jarosz, D.F., Kowalko, J.E., Yoshizawa, M., Jeffery, W.R., Borowsky, R.L., Lindquist, S., and Tabin, C.J. (2013). Cryptic Variation in Morphological Evolution: HSP90 as a Capacitor for Loss of Eyes in Cavefish. Science *342*, 1372–1375. 10.1126/science.1240276.

15. Rutherford, S.L., and Lindquist, S. (1998). Hsp90 as a capacitor for morphological evolution. Nature *396*, 336–342. 10.1038/24550.

16. Sangster, T.A., Salathia, N., Lee, H.N., Watanabe, E., Schellenberg, K., Morneau, K., Wang, H., Undurraga, S., Queitsch, C., and Lindquist, S. (2008). HSP90-buffered genetic variation is common in Arabidopsis thaliana. Proc. Natl. Acad. Sci. *105*, 2969–2974. 10.1073/pnas.0712210105.

17. Xu, Y., Singer, M.A., and Lindquist, S. (1999). Maturation of the tyrosine kinase c-src as a kinase and as a substrate depends on the molecular chaperone Hsp90. Proc. Natl. Acad. Sci. *96*, 109–114. 10.1073/pnas.96.1.109.

18. Chen, B., and Wagner, A. (2012). Hsp90 is important for fecundity, longevity, and buffering of cryptic deleterious variation in wild fly populations. BMC Evol. Biol. *12*, 25. 10.1186/1471-2148-12-25.

19. Costanzo, M., VanderSluis, B., Koch, E.N., Baryshnikova, A., Pons, C., Tan, G., Wang, W., Usaj, M., Hanchard, J., Lee, S.D., et al. (2016). A global genetic interaction network maps a wiring diagram of cellular function. Science *353*, aaf1420. 10.1126/science.aaf1420.

20. McClellan, A.J., Xia, Y., Deutschbauer, A.M., Davis, R.W., Gerstein, M., and Frydman, J. (2007). Diverse Cellular Functions of the Hsp90 Molecular Chaperone Uncovered Using Systems Approaches. Cell *131*, 121–135. 10.1016/j.cell.2007.07.036.

21. Jarosz, D.F., and Lindquist, S. (2010). Hsp90 and Environmental Stress Transform the Adaptive Value of Natural Genetic Variation. Science *330*, 1820–1824. 10.1126/science.1195487.

22. Sahni, N., Yi, S., Taipale, M., Fuxman Bass, J.I., Coulombe-Huntington, J., Yang, F., Peng, J., Weile, J., Karras, G.I., Wang, Y., et al. (2015). Widespread Macromolecular Interaction Perturbations in Human Genetic Disorders. Cell *161*, 647–660. 10.1016/j.cell.2015.04.013.

23. Schopf, F.H., Biebl, M.M., and Buchner, J. (2017). The HSP90 chaperone machinery. Nat. Rev. Mol. Cell Biol. *18*, 345–360. 10.1038/nrm.2017.20.

24. Jakobson, C.M., and Jarosz, D.F. (2019). Molecular Origins of Complex Heritability in Natural Genotype-to-Phenotype Relationships. Cell Syst. *8*, 363-379.e3. 10.1016/j.cels.2019.04.002.

25. She, R., and Jarosz, D.F. (2018). Mapping Causal Variants with Single-Nucleotide Resolution Reveals Biochemical Drivers of Phenotypic Change. Cell *172*, 478-490.e15. 10.1016/j.cell.2017.12.015.

26. Liti, G., Carter, D.M., Moses, A.M., Warringer, J., Parts, L., James, S.A., Davey, R.P., Roberts, I.N., Burt, A., Koufopanou, V., et al. (2009). Population genomics of domestic and wild yeasts. Nature *458*, 337–341. 10.1038/nature07743.

27. Peter, J., Chiara, M.D., Friedrich, A., Yue, J.-X., Pflieger, D., Bergström, A., Sigwalt, A., Barre, B., Freel, K., Llored, A., et al. (2018). Genome evolution across 1,011 Saccharomyces cerevisiae isolates. Nature, 1. 10.1038/s41586-018-0030-5.

28. Sharon, E., Chen, S.-A.A., Khosla, N.M., Smith, J.D., Pritchard, J.K., and Fraser, H.B. (2018). Functional Genetic Variants Revealed by Massively Parallel Precise Genome Editing. Cell. 10.1016/j.cell.2018.08.057.

29. Gong, Y., Kakihara, Y., Krogan, N., Greenblatt, J., Emili, A., Zhang, Z., and Houry, W.A. (2009). An atlas of chaperone–protein interactions in Saccharomyces cerevisiae: implications to protein folding pathways in the cell. Mol. Syst. Biol. *5*, 275. 10.1038/msb.2009.26.

30. Girstmair, H., Tippel, F., Lopez, A., Tych, K., Stein, F., Haberkant, P., Schmid, P.W.N., Helm, D., Rief, M., Sattler, M., et al. (2019). The Hsp90 isoforms from S. cerevisiae differ in structure, function and client range. Nat. Commun. *10*, 3626. 10.1038/s41467-019-11518-w.

31. Mok, J., Kim, P.M., Lam, H.Y.K., Piccirillo, S., Zhou, X., Jeschke, G.R., Sheridan, D.L., Parker, S.A., Desai, V., Jwa, M., et al. (2010). Deciphering protein kinase specificity through large-scale analysis of yeast phosphorylation site motifs. Sci. Signal. *3*, ra12. 10.1126/scisignal.2000482.

32. Rossi, M.J., Kuntala, P.K., Lai, W.K.M., Yamada, N., Badjatia, N., Mittal, C., Kuzu, G., Bocklund, K., Farrell, N.P., Blanda, T.R., et al. (2021). A high-resolution protein architecture of the budding yeast genome. Nature *592*, 309–314. 10.1038/s41586-021-03314-8.

33. Jakobson, C.M., She, R., and Jarosz, D.F. (2019). Pervasive function and evidence for selection across standing genetic variation in S. cerevisiae. Nat. Commun. *10*, 1222. 10.1038/s41467-019-09166-1.

34. Török, T., Mortimer, R.K., Romano, P., Suzzi, G., and Polsinelli, M. (1996). Quest for wine yeasts—An old story revisited. J. Ind. Microbiol. *17*, 303–313. 10.1007/BF01574705.

35. McCullough, M.J., Clemons, K.V., Farina, C., McCusker, J.H., and Stevens, D.A. (1998). Epidemiological investigation of vaginal Saccharomyces cerevisiae isolates by a genotypic method. J. Clin. Microbiol. *36*, 557–562.

36. Sharma, S.V., Agatsuma, T., and Nakano, H. (1998). Targeting of the protein chaperone, HSP90, by the transformation suppressing agent, radicicol. Oncogene *16*, 2639–2645. 10.1038/sj.onc.1201790.

37. Sarbassov, D.D., Ali, S.M., Kim, D.-H., Guertin, D.A., Latek, R.R., Erdjument-Bromage, H., Tempst, P., and Sabatini, D.M. (2004). Rictor, a novel binding partner of mTOR, defines a rapamycin-insensitive and raptor-independent pathway that regulates the cytoskeleton. Curr. Biol. CB *14*, 1296–1302. 10.1016/j.cub.2004.06.054.

38. Ho, P.-W., Piampongsant, S., Gallone, B., Del Cortona, A., Peeters, P.-J., Reijbroek, F., Verbaet, J., Herrera, B., Cortebeeck, J., Nolmans, R., et al. (2021). Massive QTL analysis identifies pleiotropic genetic determinants for stress resistance, aroma formation, and ethanol, glycerol and isobutanol production in Saccharomyces cerevisiae. Biotechnol. Biofuels *14*, 211. 10.1186/s13068-021-02059-w.

39. Gibson, G. (2009). Decanalization and the origin of complex disease. Nat. Rev. Genet. *10*, 134–140. 10.1038/nrg2502.

40. Paaby, A.B., and Rockman, M.V. (2014). Cryptic genetic variation, evolution's hidden substrate. Nat. Rev. Genet. *15*, 247–258. 10.1038/nrg3688.

41. Greig, D., and Leu, J.-Y. (2009). Natural history of budding yeast. Curr. Biol. *19*, R886–R890. 10.1016/j.cub.2009.07.037.

42. Loewith, R., Jacinto, E., Wullschleger, S., Lorberg, A., Crespo, J.L., Bonenfant, D., Oppliger, W., Jenoe, P., and Hall, M.N. (2002). Two TOR Complexes, Only One of which Is Rapamycin Sensitive, Have Distinct Roles in Cell Growth Control. Mol. Cell *10*, 457–468. 10.1016/S1097-2765(02)00636-6.

43. Gaubitz, C., Oliveira, T.M., Prouteau, M., Leitner, A., Karuppasamy, M., Konstantinidou, G., Rispal, D., Eltschinger, S., Robinson, G.C., Thore, S., et al. (2015). Molecular Basis of the Rapamycin Insensitivity of Target Of Rapamycin Complex 2. Mol. Cell *58*, 977–988. 10.1016/j.molcel.2015.04.031.

44. Jumper, J., Evans, R., Pritzel, A., Green, T., Figurnov, M., Ronneberger, O., Tunyasuvunakool, K., Bates, R., Žídek, A., Potapenko, A., et al. (2021). Highly accurate protein structure prediction with AlphaFold. Nature *596*, 583–589. 10.1038/s41586-021-03819-2.

45. Whitesell, L., Mimnaugh, E.G., De Costa, B., Myers, C.E., and Neckers, L.M. (1994). Inhibition of heat shock protein HSP90-pp60v-src heteroprotein complex formation by benzoquinone ansamycins: essential role for stress proteins in oncogenic transformation. Proc. Natl. Acad. Sci. U. S. A. *91*, 8324–8328. 10.1073/pnas.91.18.8324.

46. Karst, F., and Lacroute, F. (1977). Ergosterol biosynthesis inSaccharomyces cerevisiae. Mol. Gen. Genet. MGG *154*, 269–277. 10.1007/BF00571282.

47. Müller, F.-M.C., Staudigel, A., Salvenmoser, S., Tredup, A., Miltenberger, R., and Herrmann, J.V. (2007). Cross-Resistance to Medical and Agricultural Azole Drugs in Yeasts from the Oropharynx of Human Immunodeficiency Virus Patients and from Environmental Bavarian Vine Grapes. Antimicrob. Agents Chemother. *51*, 3014–3016. 10.1128/aac.00459-07.

48. Fisher, M.C., Alastruey-Izquierdo, A., Berman, J., Bicanic, T., Bignell, E.M., Bowyer, P., Bromley, M., Brüggemann, R., Garber, G., Cornely, O.A., et al. (2022). Tackling the emerging threat of antifungal resistance to human health. Nat. Rev. Microbiol. *20*, 557–571. 10.1038/s41579-022-00720-1.

49. Freeberg, M.A., Han, T., Moresco, J.J., Kong, A., Yang, Y.-C., Lu, Z.J., Yates, J.R., and Kim, J.K. (2013). Pervasive and dynamic protein binding sites of the mRNA transcriptome in Saccharomyces cerevisiae. Genome Biol. *14*, R13. 10.1186/gb-2013-14-2-r13.

50. Yan, H., Yuan, W., Velculescu, V.E., Vogelstein, B., and Kinzler, K.W. (2002). Allelic Variation in Human Gene Expression. Science *297*, 1143–1143. 10.1126/science.1072545.

51. Metzl-Raz, E., Kafri, M., Yaakov, G., Soifer, I., Gurvich, Y., and Barkai, N. (2017). Principles of cellular resource allocation revealed by condition-dependent proteome profiling. eLife *6*, e28034. 10.7554/eLife.28034.

52. Genest, O., Wickner, S., and Doyle, S.M. (2019). Hsp90 and Hsp70 chaperones: Collaborators in protein remodeling. J. Biol. Chem. *294*, 2109–2120. 10.1074/jbc.REV118.002806.

53. Wegele, H., Wandinger, S.K., Schmid, A.B., Reinstein, J., and Buchner, J. (2006). Substrate transfer from the chaperone Hsp70 to Hsp90. J. Mol. Biol. *356*, 802–811. 10.1016/j.jmb.2005.12.008.

54. Cherry, J.M., Hong, E.L., Amundsen, C., Balakrishnan, R., Binkley, G., Chan, E.T., Christie, K.R., Costanzo, M.C., Dwight, S.S., Engel, S.R., et al. (2012). Saccharomyces Genome Database: the genomics resource of budding yeast. Nucleic Acids Res. *40*, D700–D705. 10.1093/nar/gkr1029.

55. Millson, S.H., Truman, A.W., and Piper, P.W. (2022). Hsp90 and phosphorylation of the Slt2(Mpk1) MAP kinase activation loop are essential for catalytic, but not non-catalytic, Slt2-mediated transcription in yeast. Cell Stress Chaperones *27*, 295–304. 10.1007/s12192-022-01274-0.

56. Iconomou, M., and Saunders, D.N. (2016). Systematic approaches to identify E3 ligase substrates. Biochem. J. *473*, 4083–4101. 10.1042/BCJ20160719.

57. Cohen, J.D., Goldenthal, M.J., Buchferer, B., and Marmur, J. (1984). Mutational analysis of the MAL1 locus of Saccharomyces: identification and functional characterization of three genes. Mol. Gen. Genet. MGG *196*, 208–216. 10.1007/BF00328052.

58. Snoek, T., Voordeckers, K., and Verstrepen, K.J. (2014). Subtelomeric Regions Promote Evolutionary Innovation of Gene Families in Yeast. In Subtelomeres (Springer, Berlin, Heidelberg), pp. 39–70. 10.1007/978-3-642-41566-1_3.

59. Doughty, T.W., Domenzain, I., Millan-Oropeza, A., Montini, N., de Groot, P.A., Pereira, R., Nielsen, J., Henry, C., Daran, J.-M.G., Siewers, V., et al. (2020). Stress-induced expression is enriched for evolutionarily young genes in diverse budding yeasts. Nat. Commun. *11*, 2144. 10.1038/s41467-020-16073-3.

60. Domingo, J., Baeza-Centurion, P., and Lehner, B. (2019). The Causes and Consequences of Genetic Interactions (Epistasis). Annu. Rev. Genomics Hum. Genet. *20*, 433–460. 10.1146/annurev-genom-083118-014857.

61. Aguirre, L., Hendelman, A., Hutton, S.F., McCandlish, D.M., and Lippman, Z.B. (2023). Idiosyncratic and dose-dependent epistasis drives variation in tomato fruit size. Science *382*, 315–320. 10.1126/science.adi5222.

62. Jakobson, C.M., and Jarosz, D.F. (2020). What Has a Century of Quantitative Genetics Taught Us About Nature's Genetic Toolkit? Annu. Rev. Genet. *54*, 19.1-19.26. 10.1146/annurev-genet-021920-102037.

63. Smith, J.D., Suresh, S., Schlecht, U., Wu, M., Wagih, O., Peltz, G., Davis, R.W., Steinmetz, L.M., Parts, L., and St.Onge, R.P. (2016). Quantitative CRISPR interference screens in yeast identify chemical-genetic interactions and new rules for guide RNA design. Genome Biol. *17*, 45. 10.1186/s13059-016-0900-9.

64. Ohnuki, S., and Ohya, Y. (2018). High-dimensional single-cell phenotyping reveals extensive haploinsufficiency. PLOS Biol. *16*, e2005130. 10.1371/journal.pbio.2005130.

65. Karczewski, K.J., Francioli, L.C., Tiao, G., Cummings, B.B., Alföldi, J., Wang, Q., Collins, R.L., Laricchia, K.M., Ganna, A., Birnbaum, D.P., et al. (2020). The mutational constraint spectrum quantified from variation in 141,456 humans. Nature *581*, 434–443. 10.1038/s41586-020-2308-7.

66. Sarel-Gallily, R., Golan-Lev, T., Yilmaz, A., Sagi, I., and Benvenisty, N. (2022). Genome-wide analysis of haploinsufficiency in human embryonic stem cells. Cell Rep. *38*, 110573. 10.1016/j.celrep.2022.110573.

67. Echeverría, P.C., Bernthaler, A., Dupuis, P., Mayer, B., and Picard, D. (2011). An Interaction Network Predicted from Public Data as a Discovery Tool: Application to the Hsp90 Molecular Chaperone Machine. PLOS ONE *6*, e26044. 10.1371/journal.pone.0026044.

68. Chakrabortee, S., Byers, J.S., Jones, S., Garcia, D.M., Bhullar, B., Chang, A., She, R., Lee, L., Fremin, B., Lindquist, S., et al. (2016). Intrinsically Disordered Proteins Drive Emergence and Inheritance of Biological Traits. Cell *167*, 369-381.e12. 10.1016/j.cell.2016.09.017.

69. Lachowiec, J., Lemus, T., Thomas, J.H., Murphy, P.J.M., Nemhauser, J.L., and Queitsch, C. (2013). The Protein Chaperone HSP90 Can Facilitate the Divergence of Gene Duplicates. Genetics *193*, 1269–1277. 10.1534/genetics.112.148098.

70. Alvarez-Ponce, D., Aguilar-Rodríguez, J., and Fares, M.A. (2019). Molecular Chaperones Accelerate the Evolution of Their Protein Clients in Yeast. Genome Biol. Evol. *11*, 2360–2375. 10.1093/gbe/evz147.

71. Wagih, O., and Parts, L. (2014). gitter: a robust and accurate method for quantification of colony sizes from plate images. G3 Bethesda Md *4*, 547–552. 10.1534/g3.113.009431.

72. Bray, N.L., Pimentel, H., Melsted, P., and Pachter, L. (2016). Near-optimal probabilistic RNA-seq quantification. Nat. Biotechnol. *34*, 525–527. 10.1038/nbt.3519.

73. Danecek, P., Bonfield, J.K., Liddle, J., Marshall, J., Ohan, V., Pollard, M.O., Whitwham, A., Keane, T., McCarthy, S.A., Davies, R.M., et al. (2021). Twelve years of SAMtools and BCFtools. GigaScience *10*, giab008. 10.1093/gigascience/giab008.

74. Nagalakshmi, U., Wang, Z., Waern, K., Shou, C., Raha, D., Gerstein, M., and Snyder, M. (2008). The Transcriptional Landscape of the Yeast Genome Defined by RNA Sequencing. Science *320*, 1344–1349. 10.1126/science.1158441.

75. Zhao, R., Davey, M., Hsu, Y.-C., Kaplanek, P., Tong, A., Parsons, A.B., Krogan, N., Cagney, G., Mai, D., Greenblatt, J., et al. (2005). Navigating the Chaperone Network: An Integrative Map of Physical and Genetic Interactions Mediated by the Hsp90 Chaperone. Cell *120*, 715–727. 10.1016/j.cell.2004.12.024.

76. Luo, M., Meng, Z., Moroishi, T., Lin, K.C., Shen, G., Mo, F., Shao, B., Wei, X., Zhang, P., Wei, Y., et al. (2020). Heat stress activates YAP/TAZ to induce the heat shock transcriptome. Nat. Cell Biol. *22*, 1447–1459. 10.1038/s41556-020-00602-9.

77. Diezmann, S., Michaut, M., Shapiro, R.S., Bader, G.D., and Cowen, L.E. (2012). Mapping the Hsp90 genetic interaction network in Candida albicans reveals environmental contingency and rewired circuitry. PLoS Genet. *8*, e1002562. 10.1371/journal.pgen.1002562.

78. The UniProt Consortium (2023). UniProt: the Universal Protein Knowledgebase in 2023. Nucleic Acids Res. *51*, D523–D531. 10.1093/nar/gkac1052.